

The evolution of dystonia-like movements in TOR1A rats after transient nerve injury is accompanied by dopaminergic dysregulation and abnormal oscillatory activity of a central motor network

Susanne Knorr^a, Lisa Rauschenberger^a, Uri Ramirez Pasos^a, Maximilian U. Friedrich^a, Robert L. Peach^a, Kathrin Grundmann-Hauser^{b,c}, Thomas Ott^{b,d}, Aet O'Leary^e, Andreas Reif^e, Philip Tovote^f, Jens Volkmann^a, Chi Wang Ip^{a,*}

^a Department of Neurology, University Hospital of Würzburg, 97080, Germany

^b Institute for Medical Genetics and Applied Genomics, University of Tübingen, 72076, Germany

^c Centre for Rare Diseases, University of Tübingen, 72076, Germany

^d Core Facility Transgenic Animals, University Hospital of Tübingen, 72076, Germany

^e Department of Psychiatry, Psychosomatic Medicine, and Psychotherapy, University Hospital Frankfurt, 60528, Germany

^f Systems Neurobiology, Institute of Clinical Neurobiology, University Hospital of Würzburg, Versbacher Straße 5, 97080, Germany

ARTICLE INFO

Keywords:

DYT1
TOR1A
Two-hit hypothesis
Dopamine
LFP

ABSTRACT

TOR1A is the most common inherited form of dystonia with still unclear pathophysiology and reduced penetrance of 30–40%. Δ ETorA rats mimic the TOR1A disease by expression of the human TOR1A mutation without presenting a dystonic phenotype. We aimed to induce dystonia-like symptoms in male Δ ETorA rats by peripheral nerve injury and to identify central mechanism of dystonia development. Dystonia-like movements (DLM) were assessed using the tail suspension test and implementing a pipeline of deep learning applications. Neuron numbers of striatal parvalbumin⁺, nNOS⁺, calretinin⁺, ChAT⁺ interneurons and Nissl⁺ cells were estimated by unbiased stereology. Striatal dopaminergic metabolism was analyzed via in vivo microdialysis, qPCR and western blot. Local field potentials (LFP) were recorded from the central motor network. Deep brain stimulation (DBS) of the entopeduncular nucleus (EP) was performed. Nerve-injured Δ ETorA rats developed long-lasting DLM over 12 weeks. No changes in striatal structure were observed. Dystonic-like Δ ETorA rats presented a higher striatal dopaminergic turnover and stimulus-induced elevation of dopamine efflux compared to the control groups. Higher LFP theta power in the EP of dystonic-like Δ ETorA compared to wt rats was recorded. Chronic EP-DBS over 3 weeks led to improvement of DLM. Our data emphasizes the role of environmental factors in TOR1A symptomatogenesis. LFP analyses indicate that the pathologically enhanced theta power is a physiological marker of DLM. This TOR1A model replicates key features of the human TOR1A pathology on multiple biological levels and is therefore suited for further analysis of dystonia pathomechanism.

1. Introduction

The dystonias are a family of heterogeneous disorders affecting more than 3 million people worldwide. They share the commonality of involuntary, abnormal focal or generalized movements or postures caused by sustained or intermittent muscle contractions, but may be caused by a variety of genetic or extragenetic factors. This has prompted the search for common final pathophysiological pathways, which may express the same phenotype despite divergent etiopathogeneses.

Current concepts of dystonia pathophysiology emphasize three general abnormalities: loss of inhibition, sensory dysfunction and alterations in synaptic plasticity (Balint et al., 2018; Quartarone and Hallett, 2013). These abnormalities are thought to contribute to a central sensorimotor network dysfunction involving the basal ganglia-motor circuit and possibly the cerebellum (Balint et al., 2018), which is hallmarked by abnormal oscillatory activity (Neumann et al., 2017) and results in dystonic symptoms such as abnormal involuntary muscle contractions and postures, dystonic overflow and abnormal sensation (Conte et al.,

* Corresponding author at: Department of Neurology, University Hospital of Würzburg, Josef-Schneider-Straße 11, 97080 Würzburg, Germany.

E-mail address: ip_c@ukw.de (C.W. Ip).

<https://doi.org/10.1016/j.nbd.2021.105337>

Received 7 January 2021; Received in revised form 8 March 2021; Accepted 17 March 2021

Available online 19 March 2021

0969-9961/© 2021 The Author(s).

Published by Elsevier Inc.

This is an open access article under the CC BY-NC-ND license

(<http://creativecommons.org/licenses/by-nc-nd/4.0/>).

2019). While no overt structural abnormalities have so far been identified in the central nervous system of isolated dystonia, imaging studies have revealed subtle microstructural and metabolic changes in non-manifesting as well as manifesting TOR1A mutation carriers (Carbon et al., 2004; Carbon et al., 2009). TOR1A (also called DYT-TOR1A, DYT1) is the most common inherited form of isolated, generalized dystonia caused by a trinucleotide GAG in-frame deletion (Δ GAG, Δ E) in the TOR1A gene, encoding for the AAA+ ATPase torsinA. The notion that the brain of TOR1A mutation carriers might already present abnormalities in the sense of an endophenotype before symptom onset, was further supported by reports on impaired motor learning in TOR1A mutation carriers (Carbon et al., 2011; Ghilardi et al., 2003). Previous studies on the neurobiology of torsinA have suggested a role in dopaminergic transmission and in the cellular response to stress (Augood et al., 2002; Hewett et al., 2003). However, through which mechanisms the genetic defect causes overt dystonia along the complex path from protein abnormality, to cellular dysfunction and micro- or large-scale circuit disorder remains enigmatic.

Because disease penetrance is reduced to 30–40%, the torsinA defect seems to be a necessary, albeit not sufficient precondition for overt dystonia. The D216H TOR1A polymorphism has been described as genetic modifier, but explains only a small proportion of the reduced penetrance (Risch et al., 2007). Possible extragenetic factors such as perinatal adversities, previous childhood infections, prior general anaesthesia or physical trauma were investigated in a recent retrospective review of 28 families with TOR1A dystonia. Despite the inherent problems of insufficient power and retrospective assessment, the survey revealed a significant association with perinatal adversity as an environmental factor influencing penetrance (Martino et al., 2013).

In this study, we set out to provide experimental evidence for a relevant interaction between genetic predisposition and physical trauma in the symptomatology of TOR1A dystonia. Here, we explore the induction of a dystonic phenotype in a transgenic TOR1A rat model (Tgh Δ GAGTorA18; Δ ETorA) through a peripheral nerve trauma as a way to trigger maladaptive plasticity in a susceptible brain. The Δ ETorA rat model overexpresses the human, mutated TOR1A gene, but presents no dystonic phenotype per se (Grundmann et al., 2012). To elucidate disease mechanism, we provide longitudinal behavioral assessments and analyze structural, neurotransmitter and large-scale network changes focussing on the basal ganglia in relation to genotype and phenotype. Finally, we probe therapeutic effects of deep brain stimulation (DBS) of the entopeduncular nucleus (EP) in Δ ETorA rats.

2. Materials and methods

2.1. Animals

74 male transgenic hemizygous Δ ETorA rats and 70 male wild type (wt) littermates on Sprague–Dawley background, 12 weeks old, were bred in the animal facility of Tübingen and kept under standard conditions (21 °C, 12-h light/dark cycle). Determination of the genotype was performed as previously described (Grundmann et al., 2012). All applicable international, national, and/or institutional guidelines for care and use of animals were followed. All animal experiments were approved by the local government.

2.2. Sciatic nerve crush injury

Deeply isoflurane-anesthetized rats received a right-sided sciatic nerve crush injury for 30 s or sham surgery, performed as previously described (Ip et al., 2016).

2.3. Behavioral studies by tail suspension test

Blinded behavioral assessments of videorecordings (recording and observing person were blinded to genotype and crush injury) were

conducted at baseline (pre OP) and after nerve crush or sham injury (week 2, 5, 9 and 12). Rats were suspended by their tail, intervals of 30 s were recorded and analyzed with a scoring system modified after Ip et al. for the evaluation of DLM observed in the hindlimbs (Ip et al., 2016): 0–4 point score (Table 1): no abnormal movements (0), short hindlimb and retraction of <3 s or ≤ 2 repeats (1), hindlimb retraction and clenching of ≥ 3 s to <10 s or ≥ 3 repeats (2), hindlimb retraction and clenching of 10 s or $<50\%$ of the recorded time (3), hindlimb retraction and clenching of $\geq 50\%$ of the recorded time (4).

2.4. Deep neural networks for markerless pose estimation

For quantitative analysis of motor behavior, the deep learning framework DeepLabCut (DLC) was utilized (Mathis et al., 2018). This tool implements a convolutional neural network consisting of a residual neural network (ResNet) and deconvolutional layers whose feature detectors are fine-tuned in a supervised manner by adding user annotated data containing the locations of the bodyparts to be tracked. We implemented a pretrained network on 400 frames of rodents (from an independent experimental batch of TOR1A rodents from another dystonia project) undergoing tail suspension tests that was extended with another 142 distinct frames from standardized videos (10 s duration each, resolution of 50 frames per second) of rats from the current project undergoing the tail suspension test. 7–10 frames/video were extracted using the DLC included “k-Means” and “uncertain” functions, on which consequently 31 bodyparts mainly comprising the trunk, tail and both hindlimbs were manually labeled and defined as the skeleton by a rater blinded to the animals’ condition (Fig. 3A,C, suppl. Movie S2). To ensure high labelling accuracy, the labeled frames were plotted and visually inspected before the network was trained on 95% of the total frames, retaining the remainder as a test set for performance evaluation. For the training, default augmentation and ResNet50’s initialization weights were chosen, while the number of iterations ranged between 500,000 and 850,000, making sure the loss function sufficiently converged. After iteratively refining the network two times according to the workflow proposed (Nath et al., 2019), its performance was evaluated by calculating the train/test error as measured by the mean euclidean distance of the user’s and the network’s predicted label positions above the likelihood threshold of 0.6, which yielded 2.3 and 8.9 pixels, respectively. Given the average dimension of a rat paw projecting onto 120×90 pixels (L x W) in the video material, the error was deemed acceptably small so that the neural network was then used for analyzing videos.

Two-dimensional coordinate time series data (approximately 1500 frames length) of nerve-injured wt and Δ ETorA rats undergoing the tail suspension test on week 9 and 12 were collected via the DLC video analysis function, batch imported into R Studio (R Core Team: <https://www.R-project.org/>) and preprocessed as to exclude predictions below a likelihood threshold of 0.6. Single missing coordinates ($<3\%$, i. e. $<40/1500$ frames per bodypart) were imputed using a linear approximation function per column. Subsequently, the time series were aggregated and standardized by z-score transformation in order to homogenize inherently differently scaled vector length, angular and correlation data to prevent artificial clustering in further analyzes. 76 features (e. g. angles, vector lengths, their descriptives and correlations) reflecting the visual scoring criteria and in addition several other kinematic parameters allowing comprehensive description of truncal, hindlimb and hindpaw movements, were derived from the aggregated time series using built-in R functions.

Given the ratio of the sample size and the number of presumably partly collinear features, two strategies for dimensionality reduction and feature selection were implemented to prevent overfitting in classification models. An intrinsic stepwise variable selection algorithm feeding into a 5-fold cross-validated quadratic linear discriminant analysis (QDA) function (MASS package for R: <https://CRAN.R-project.org/package=MASS>) was used to assess predictors for the genotype, which were evaluated by feature wise calculation of the area under the receiver

Table 1
Scoring system for DLM in hindlimbs after peripheral nerve crush modified after Ip et al., 2016.

Dystonia-like movement (DLM) scoring system.				
0	1	2	3	4
DLM score	DLM score	DLM score	DLM score	DLM score
no DLM	short hindlimb retraction and clenching <3 s or ≤2 repeats	hindlimb retraction and clenching ≥3 s to <10 s or ≥3 repeats	hindlimb retraction and clenching 10 s to <50% of the recorded time	hindlimb retraction and clenching ≥50% of the recorded time

operating curves (AUROC). In line with theoretical considerations pertaining to the optimal feature/sample ratio, the 10 largest coefficients of a linear support vector machine with 10-fold randomized cross-validation (e1071 package for R: <https://CRAN.R-project.org/package=e1071>) were further explored. Systematic examination of feature combinations, tuning of hyperparameters to reduce the feature space and to optimize variance-bias trade-off in various data perturbations resulted in four optimal features (Fig. 3A). As an unsupervised cross-validation approach, a k-Means cluster analysis (k-clusters = 2) using the Lloyd algorithm and 20 random initialisations as supplied in R was conducted on both Z-score transformed week 9 and week 12 subsets of the data.

2.5. Nerve conduction studies

Recordings of compound muscle action potentials (CMAP) and nerve conduction velocities (NCV) were performed in isoflurane-anesthetized rats with a digital Neurosoft-Evidence 3102 electromyograph (Schreiber & Tholen Medizintechnik, Stade, Germany) using steel needle electrodes as described (Ip et al., 2016).

2.6. Histology and immunohistochemistry

After transcardial perfusion with 4% paraformaldehyde, tissue was incubated in 30% sucrose, embedded in Tissue-Tek O.C.T and cryocut into 40 µm-thick coronal serial-sections of the striatum (2.7 to -4.1 mm relative to bregma). Series of free-floating sections were stained for parvalbumin (PV, Ab11427, Abcam, Cambridge, UK), neuronal nitric oxide synthase (nNOS, 24,431, ImmunoStar, Hudson, USA), calretinin (CR) and choline acetyltransferase (ChAT)(CR: MAB1568; ChAT: AB144P, Merck Millipore, Burlington, USA). For Nissl staining, sections were incubated in 0.1% cresyl violet solution for 30 min, rinsed in aqua bidest, dehydrated in an ascending ethanol series and incubated in xylene.

2.7. Stereology

Unbiased stereology was performed with the Olympus BX53 microscope, a 100×/1.25 numerical aperture objective and the StereoInvestigator software (version 11.07; MicroBrightField Biosciences, Williston, VT) using these settings: Sections separated by 480 µm (1/12 series), counting frame 60 × 60 µm, grid size 160 × 160 µm (PV⁺), 120 × 120 µm (CR⁺), 100 × 100 µm (nNOS⁺ and ChAT⁺) neurons; Nissl⁺ cells counting frame 20 × 20 µm, grid size 600 × 600 µm, guard zone 2 µm. Gundersen coefficients of error $m = 1 \leq 0.1$.

2.8. Real-time PCR (qPCR)

mRNA of snap frozen striatum was isolated with RNeasy Micro Kit (Qiagen, Hilden, Germany) and reverse transcribed to cDNA with SuperScrip IV VILO™ Master Mix (Thermo Fisher, Darmstadt, Germany) according to the guidelines of manufacturers. For gene expression analysis TaqMan® assay (*Darpp32*: Rn01452984_m1, *Drd1*: Rn03062203_s1, *Drd2*: Rn00561126_m1, *Drd3*: Rn00567568_m1, *Drd4*: Rn00681263_g1, *Drd5*: Rn00562768_s1, *Gapdh*: Rn99999916_s1) and

TaqMan Gene Expression Master Mix were used. Triplicates were performed and analyzed by the $2^{-\Delta\Delta CT}$ method. Results were normalized to the control wt group.

2.9. In vivo microdialysis

24 h before microdialysis onset, self-made microdialysis probes (3 mm active tip) were implanted bilaterally into the striatum of isoflurane-anesthetized rats. Coordinates: 0.7 mm AP, -7.0 mm DV, ± 3.0 mm ML. Six baseline samples were collected in freely moving rats with artificial CSF (aCSF), followed by perfusion with KCl-enriched aCSF (50 mM) for 30 min and a collection of 14 additional samples in 15-min periods each with a perfusion rate of 1.5 µl/min and stabilized with 7.5 µl of 0.02 M acetic acid. Quantification of catecholamines was based on high performance liquid chromatography (HPLC) with electrochemical detection by DECADE Elite (Antec Scientific, Zoeterwoude, Netherlands). For dopamine (DA) analysis, 10 µl of microdialysis sample was separated on a NeuroSep 115 C18 column (ERC, Munich, Germany) with a isocratic mobile phase at 42 °C and detected with a working potential of +460 mV versus ISAAC reference electrode at 42 °C. 3,4-Dihydroxyphenylacetic acid (DOPAC) and homovanillic acid (HVA) was analyzed by separating 5 µl of a microdialysis sample with a isocratic mobile phase at 37 °C and detected with a working potential of +570 mV versus ISAAC reference electrode at 37 °C. External standards were used for quantification.

2.10. Western blot

Protein lysates of snap frozen striatum were separated by a sodium-dodecyl-sulphate-polyacrylamide gel electrophoresis and transferred to nitrocellulose membrane. Primary antibodies (dopamine transporter (DAT): AB2231, Merck; DA receptor D1 (Drd1): sc-31,478, Santa Cruz Biotechnology; DA receptor D2 (Drd2): AB5084P, Merck; GAPDH: CB1001, Merck) were incubated overnight at 4 °C in TBST 5% milk. HRP-conjugated secondary antibodies were incubated for 1 h at room temperature, followed by ECL visualization. Data were analyzed with the Image Lab software (version 6.0.1, Bio-Rad, Hercules, CA, USA). DAT, Drd1 and Drd2 protein levels were normalized to the endogenous control GAPDH and to wt control animals.

2.11. Electrode implantation and DBS

Deep brain stimulation electrodes were implanted into the brain 9 weeks after nerve crush injury to the contralateral hemisphere. A monopolar platinum/iridium electrode with an impedance between 0.8 and 1.1 MΩ (UE-PSEGSECN1M; FHC Inc., Bowdoin, ME) was implanted into the EP using the coordinates:

-2.28 mm AP, -2.7 mm ML, -7.3 mm DV. Self-made monopolar platinum/iridium electrodes were implanted into the primary motor cortex (MC): 0.96 mm AP, -2.0 mm ML, -1.0 mm DV. For DBS, the EP-electrode was connected to a custom-made plug. Settings for high-frequency stimulation (HFS) of the EP were 200 µs pulse length, 130 Hz frequency and an amplitude 10% below the occurrence of side effects using the multichannel systems stimulus generator (STG 4004; Multi-channelSystems, Reutlingen, Germany). Two animals had to be

excluded from all analyses due to wrong positioning of the electrode.

2.12. LFP recordings and data collection

LFP recordings of mildly isoflurane-anesthetized rats (0.8%) were performed 9 and 12 weeks after nerve crush injury. All recordings were done in stimulation (stim) OFF state. LFP signals were amplified (x1000) and analog-filtered (0.1–1000 Hz) by an AC differential amplifier (DAM80 WPI Instruments). The data were digitized at 20 kHz (Cambridge Electronic Design (CED) 1401 micro3, Cambridge, UK) and downsampled to 1–2 kHz for analysis with recording lengths of 120 s. Reference cable connected to a silver screw placed on the nasal bone. All recordings were processed and analyzed with MATLAB (release 2016b, The MathWorks, Inc., Natick, MA, USA). To prepare signals for spectral analysis, functions from the Fieldtrip Toolbox (<http://www.ru.nl/neuroimaging/fieldtrip>) were employed (Oostenveld et al., 2011). Segments with electrical artifacts were visually identified and removed from the recordings. Signals were downsampled to 256 Hz, bandpass-filtered (cutoff frequencies 0.5 and 100 Hz) and notch-filtered (49–51 Hz) using an infinite impulse response Butterworth filter of fourth order with forward and reverse pass. Spectral power was computed using discrete prolate spheroidal sequences as tapers before performing a Fourier transformation (Oostenveld et al., 2011). Spectral smoothing was effected over ± 2 Hz and frequencies of interest were 1–100 Hz with a resolution of 0.5 Hz. Power values were normalized by the mean standard deviation of power within 5–45 Hz and 55–95 Hz to derive relative power as described for human dystonia (Neumann et al., 2017). 1/f bias was corrected by computing the slope (α) of power for each recording and multiplying power with f^α as described (Smith et al., 2015). Finally, mean relative power was computed for the theta (4–7 Hz), beta (14–35 Hz) ranges, and the frequency range of 8–20 Hz.

2.13. Statistical analysis

Statistical analysis was carried out using GraphPad Prism software (Version 8; San Diego, CA, USA). The distribution of data was analyzed by Kolmogorow-Smirnow normality test and Q-Q-plots. Comparison of four or more groups of non-normally distributed data were done with the Kruskal-Wallis-test and Dunn's multiple comparison test; a comparison of multiple groups of normally distributed data was done with a one-way ANOVA and Tukey's multiple comparison test. The Mann-Whitney test was employed for two-group comparisons of non-normally distributed data. For data with multiple time points, the Bonferroni-Holm correction was applied (§). The Chi-square test was

performed for the data of dystonia categories by body distribution. Microdialysis data were analyzed with mixed-effects model and Dunn's multiple comparisons test. Data are presented as mean \pm standard error of mean (SEM). Statistical significances were labeled as * $p < 0.05$, ** $p < 0.01$, *** $p < 0.001$, **** $p < 0.0001$, $^\psi p < 0.05$, $^\psi^\psi p < 0.01$, $^\psi^\psi^\psi p < 0.001$, $^\psi^\psi^\psi^\psi p < 0.0001$, # $p < 0.05$, ## $p < 0.01$, ### $p < 0.001$, #### $p < 0.0001$, \$ $p < 0.05$, \$\$ $p < 0.01$, \$\$\$ $p < 0.001$.

3. Results

3.1. Sciatic nerve crush injury triggers DLM in Δ E T orA rats

During tail suspension, nerve-injured rats presented repetitive, abnormal movements with retraction of the crushed hindlimb and clenching of the toes as a sign of focal DLM (Fig. 1A). Spreading of DLM to the contralateral hindlimb was observed in 35% of Δ E T orA nerve-injured animals and characterized as beginning generalized DLM (Fig. 1B). Normal posturing of hindlimbs as seen in naïve rats (Fig. 1C) and hindlimb claspings as motor abnormality (Fig. 1D), were recorded and characterized as no DLM. Duration and frequency of DLM were evaluated with a scoring system adapted from Ip et al. (Table 1, Fig. 2A) (Ip et al., 2016). 2 weeks after nerve injury, expression of DLM reached a maximum score in both wt and Δ E T orA rats and decreased continuously until week 9. However, DLM scores of nerve-injured Δ E T orA rats consistently remained on a significantly higher level from week 9 onwards compared to nerve-injured wt rats, where DLM regressed completely. Naïve and sham operated animals did not develop DLM. 40% of Δ E T orA nerve-injured animals presented with focal DLM only, 35% exhibited beginning signs of generalization of DLM to the contralateral hindlimb and 25% did not develop DLM during week 9 to 12 (average DLM scores of both timepoints) after sciatic nerve crush injury. 30% of wt crush rats developed focal DLM, 70% did not present any dystonic symptoms at all (Fig. 2B).

3.2. Discriminating kinematic features are reflective of DLM

To validate DLM data we focused on the late, DLM discriminating time points (comparing wt to Δ E T orA rats) after nerve crush injury (9 and 12 weeks) and chose a multimodal approach to feature selection by means of a variable selection algorithm/QDA and exploration of support vector classifier (SVC) coefficients, thereby revealing kinematic features reflecting DLM. Feature F1, measuring the distance of the right hindlimb to the body's medial length axis, was most discriminatory for genotype with an AUROC of 0.87 (Fig. 3A,C,E). In combination with additional

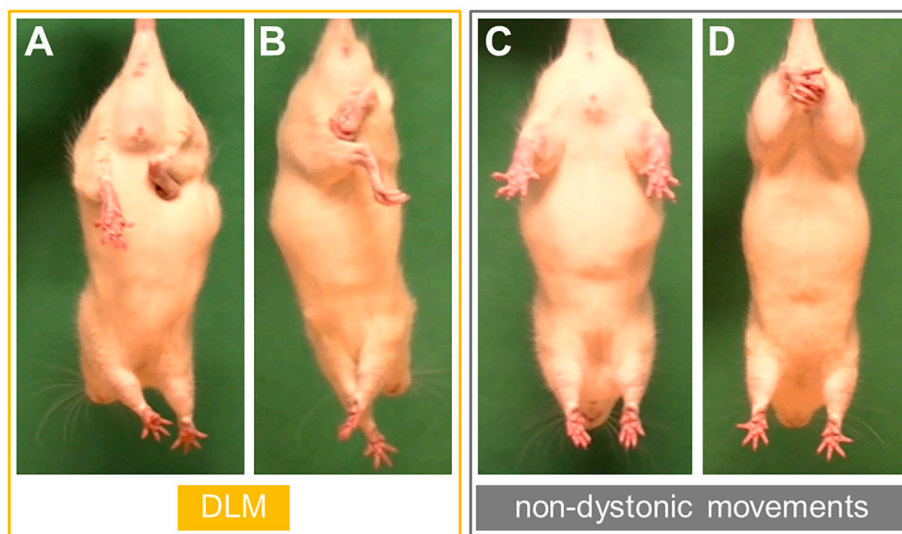


Fig. 1. DLM after peripheral nerve crush recorded during tail suspension test.

Images of DLM after unilateral nerve crush injury and images of non-dystonic movements during a tail suspension test. (A) Abnormal postures with retraction and clenching of the right foot and leg was classified as focal DLM. (B) Hindlimb retraction and clenching of the right leg with simultaneous dystonia-like adduction of the left leg crossing the body midline was scored as a beginning generalization of DLM. (C) Normal posture of hindlimbs in a naïve rat. (D) Abnormal hindlimb claspings in a naïve rat.

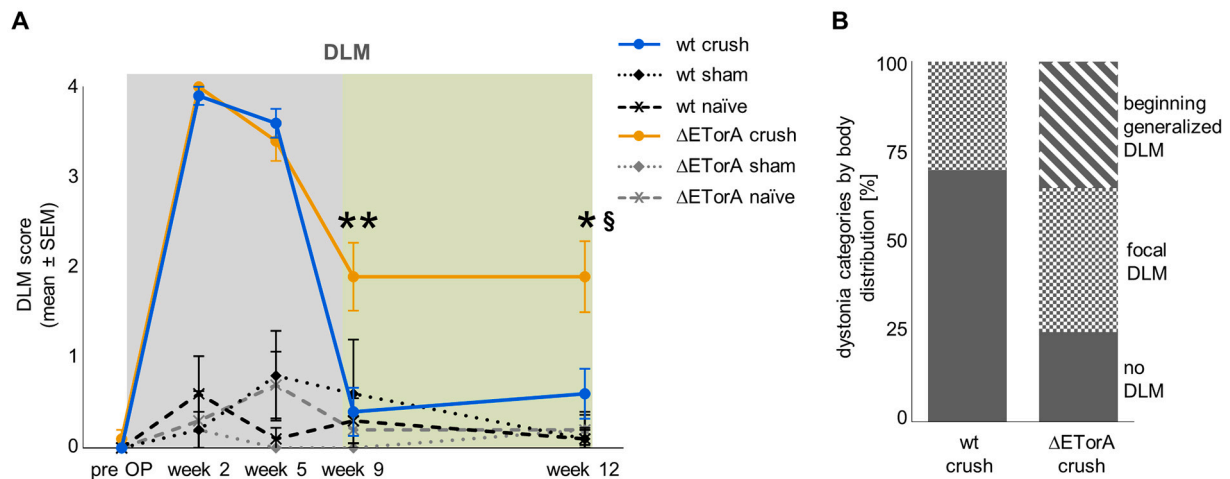


Fig. 2. Long-lasting dystonia-like phenotype induced by peripheral trauma in Δ ETorA rats.

(A) DLM seen in the hindlimbs of Δ ETorA rats (orange line, $n = 10$) and wt rats (blue line, $n = 10$) after nerve crush injury were analyzed with a scoring system modified after Ip et al., 2016 during an observational period of 12 weeks (wt naïve: black dashed line, $n = 8$; Δ ETorA naïve: grey dashed line, $n = 9$, wt sham operated: black dotted line, $n = 5$; Δ ETorA sham operated: grey dotted line, $n = 5$). (B) Based on the DLM scoring system, the distribution of dystonia in Δ ETorA and wt rats after 9 to 12 weeks (average DLM scores of both timepoints) after peripheral nerve crush was evaluated and subdivided in: no DLM (grey), focal DLM (tilled, involvement only of the nerve-injured hindlimb), beginning generalized DLM (striped, bilateral involvement of the hindlimbs). Data are shown as mean \pm SEM for each time point. Statistical analysis in A was performed with a two-tailed Mann-Whitney test comparing Δ ETorA crush and wt crush rats for each time point followed by Bonferroni-Holm correction. * $p < 0.05$ and ** $p < 0.01$ indicate significant differences between these two groups for each time point. § indicates a significant difference after Bonferroni-Holm correction of the p -values for the entire experimental period of 12 weeks. For the data of dystonia categories by body distribution (B), the Chi-square test was applied ($\chi^2(2) = 57.74, p < 0.0001$).

three features describing the relative distance of both calcanei (F2, AUROC 0.80) and toe synergisms of the left and right hindpaw as measured by intercorrelations (F3, AUROC 0.55 and F4, AUROC 0.75), an overall good classification accuracy for genotype was achieved without compromising pattern separability in the cross-validated data (Fig. 3A,C,E). In addition, DLM is visually reflected by temporally aggregated coordinate plots (CP) (Fig. 3B,D). While in CP of rats showing no DLM, hindlimb movements were clearly separated in the horizontal plane and range of movement in both the vertical and horizontal axis were of symmetrical extents (Fig. 3B), pronounced DLM demonstrate CP with lack of separability in the horizontal plane as well as an asymmetrical extent of movement in the Y plane and reduced range of motion in both planes on the right side due to proximal hindlimb crossing, retraction, and paw clenching (Fig. 3D). Interestingly, the F1-F4 features are, at least partially, reflective of the main items of the utilized DLM score, assessing spectra of hindlimb retraction (F1 & F2) and paw clenching (F3 & F4), while also potentially capturing overflow phenomena to the contralateral side (F2 & F4). With F1 & F2 measuring means, the time factor of the DLM scoring is indirectly represented, since they depict duration and extent of dystonic movements.

3.3. Kinematic analysis predicts the presence of DLM

Objective exploration of subgroups divided by the presence or absence of motor abnormalities irrespective of genetic background, i. e. subjects with DLM scores of zero vs. non-zero, by means of a two centered k-Means cluster analysis on video-extracted kinematic features confirmed strong inherent separability with a high classification accuracy of 0.85 both in the week 9 and week 12 dataset. In order to further examine the extent to which the defined kinematic feature space can depict motor abnormalities, a linear SVC was trained using week 12 data annotated with the dichotomized DLM score. This model showed classification accuracy of 0.85 on a test set of week 12 data and 0.71 when tested on additional unseen data from week 9. Factoring in genetic background as an additional covariate in the model, accuracy improved to 0.85.

3.4. Kinematic analysis predicts genotype at late stages after nerve-injury

Another two-centered k-Means cluster analysis revealed natural clustering of genotype groups (i. e. wt vs. Δ ETorA) which was classified with an accuracy of 0.85 in both week 12 and week 9 datasets. The linear SVC model trained on week 12 data grouped per genotype yielded perfect classification accuracy of 1.0 in five-fold cross-validation and 0.85 when applied to the unseen week 9 test set, underlining good generalization. Accuracy remained unchanged when factoring in the dichotomized DLM score.

3.5. Normal functional recovery of the sciatic nerve in injured Δ ETorA rats

Excluding a peripheral etiology of DLM in Δ ETorA rats, NCV and CMAP of the injured sciatic nerve did not differ comparing Δ ETorA rats with wt animals at baseline (Fig. 4A-D). Electrophysiological recordings immediately after sciatic nerve crush showed a complete conduction block confirming the efficacy of the nerve crush (Fig. 4A). 11 weeks after sciatic nerve injury the affected nerves had partially recovered, however, they still showed significantly prolonged latencies (Fig. 4A,B) and reduced CMAP (Fig. 4A,C,D) compared to baseline. No significant differences in NCV and CMAP recovery were seen comparing the injured nerves of Δ ETorA rats with wt rats, which points towards a central origin of the DLM observed in Δ ETorA rats.

3.6. Unchanged striatal neuronal cell number in Δ ETorA rats

12 weeks after sciatic nerve crush injury, the number of interneurons positive for PV, nNOS, CR and ChAT (Fig. 5A-T) and Nissl⁺ neurons did not differ between all experimental groups (Fig. 5U-Y). qPCR analysis showed no significant differences in gene expression levels of the cyclic AMP-regulated phosphoprotein *Darpp32* in the striatum, a marker of medium spiny neurons, in all experimental groups (Fig. 5Z).

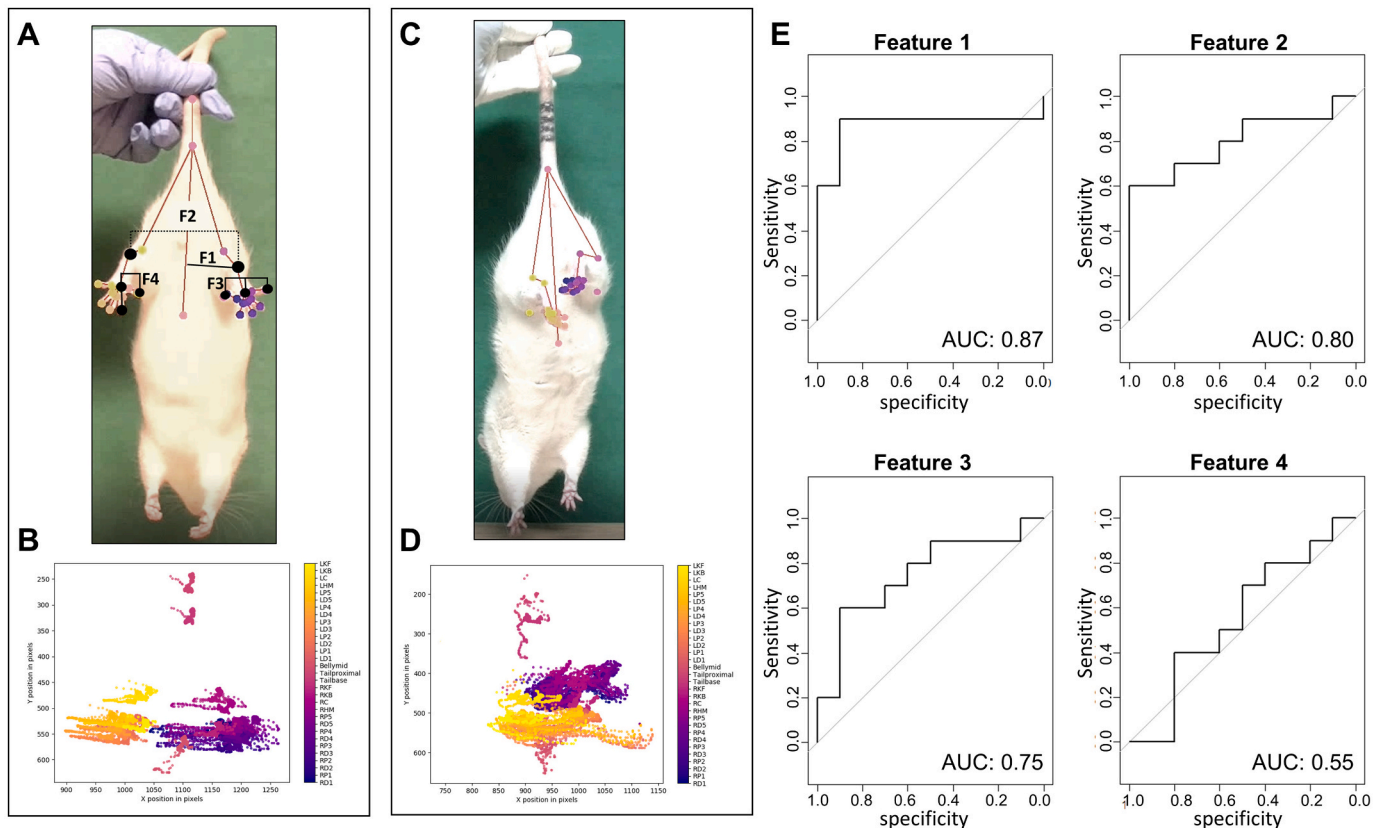


Fig. 3. Kinematic analysis using DeepLabCut validates observer-based DLM data in Δ ETorA rats.

(A,C) Markerless pose estimation of animals undergoing tail suspension test. (B,D) Respective temporally aggregated coordinate plots (CP). (A,B) Example of normal motor behavior. (C,D) Example of rat with DLM. (E) Classification accuracy for genotype assessed by feature wise calculation of the area under the receiver operating curves (AUC).

F1: mean of the distance vector from right calcaneus orthogonally projecting onto body length axis. F2: mean of the distance vector separating both calcanei. F3: correlation of distance vectors from first and fifth digits'tips to the right hand mid. F4: correlation of distance vectors from first and second digits'tips to the left hand mid. Bodyparts for CP in B and D: L and R denote left and right, D and P refer to distal and proximal, 1–5 refer to respective fingers (thumb = digit 1 asf.), C = calcaneus, K = knee.

3.7. Striatal dopaminergic dysregulation in dystonic Δ ETorA rats

We then asked whether dopamine signaling was differentially affected by nerve trauma in Δ ETorA rats. Similar baseline levels of striatal DA release were found in all groups via *in vivo* microdialysis contralateral to the peripheral nerve crush (Fig. 6A,B). An acute potassium stimulus resulted in a significant elevation of DA in Δ ETorA rats 12 weeks after subsection to the nerve injury compared to wt crush animals and both control groups. In contrast to this stress-induced effect, the level of the dopaminergic metabolite DOPAC was found to be elevated over the entire measurement period in Δ ETorA rats after sciatic nerve crush compared to both naïve control groups in the contralateral striatum (Fig. 6C). A trend, but no significance was noted for elevated DOPAC levels compared to the wt animals subjected to a nerve crush. Increased HVA expression levels were observed in both nerve-injured groups compared to naïve wt and Δ ETorA animals (Fig. 6D). Significant differences in DA turnover rates were observed only for the DOPAC/DA turnover at baseline conditions in nerve-injured Δ ETorA rats compared to the naïve control groups (Fig. 6E). Mildly but significantly elevated HVA/DA turnover rates were shown in nerve-injured Δ ETorA rats with similar levels to nerve-injured wt rats compared to naïve control animals at baseline (Fig. 6F). DAT protein levels showed a non-significant reduction after peripheral nerve crush in Δ ETorA rats compared to the Δ ETorA control group, while a slight increase for DAT was found in wt animals after crush (Fig. 6G). No significant differences in striatal DA D1 and D2 receptor protein expression in wt and Δ ETorA

rats were observed at baseline. After sciatic nerve injury a robust decline of D2 receptor protein was found in the contralateral striatum of dystonic-like Δ ETorA rats compared to their naïve counterparts ($p = 0.0567$), while D1 receptor proteins did not change significantly (Fig. 6H,I). No changes were found for the relative mRNA levels of DA receptors (*Drd1–5*) in the striatum of Δ ETorA rats compared to wt rats in their naïve state as well as 12 weeks after sciatic nerve crush injury (Fig. 6J–N).

3.8. DLM in Δ ETorA rats are associated with theta oscillations in EP and improve with DBS

After presenting a likely consequence of altered dopaminergic signaling in Δ ETorA nerve-crushed rats, we next investigated a putative pathophysiological effect on basal ganglia network function. Therefore, we performed LFP recordings from MC and EP with a focus on differences in oscillatory brain network activity between nerve-injured Δ ETorA and wt rats. Theta power was significantly higher in Δ ETorA crush rats (9 weeks) in the EP and MC compared to wt crush rats (Fig. 7A,D,E). A significantly reduced beta power was recorded in the EP in Δ ETorA rats compared to wt rats. Beta power of the MC showed a similar trend without statistically significance towards a reduction in Δ ETorA rats compared to wt rats (Fig. 7B,D,E). LFP power in the frequency range of 8–20 Hz demonstrated a significant decrease in both EP and MC of Δ ETorA crush rats (Fig. 7C,D,E).

Continuous HFS of the EP over a period of 3 weeks improved DLM

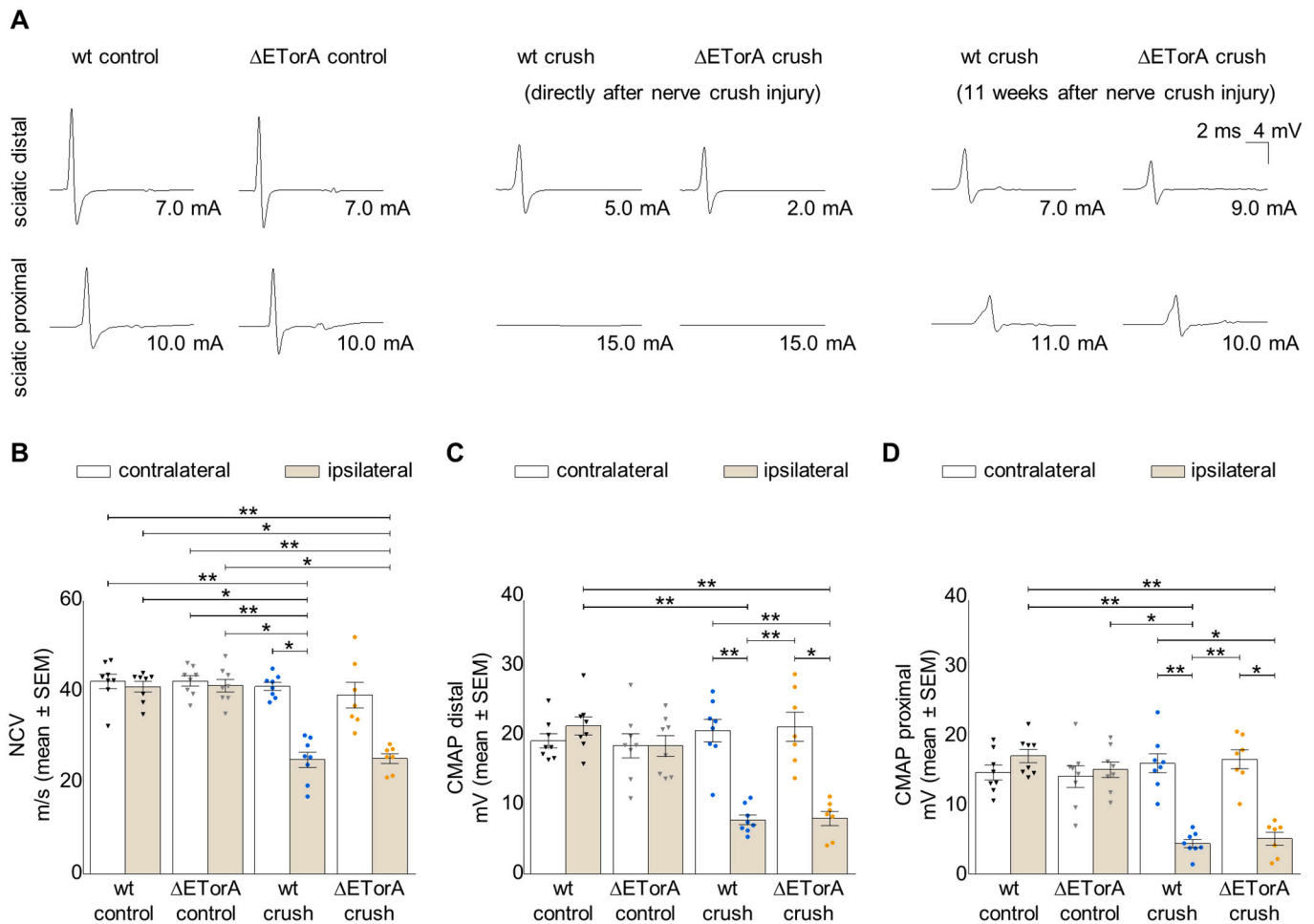


Fig. 4. Peripheral nerve regeneration after nerve-injury is similar in Δ ETorA and wt rats.

(A) Representative examples of electrophysiological recordings of the right sciatic nerve in naïve wt and Δ ETorA animals (left), in wt and Δ ETorA animals directly after peripheral nerve crush (middle) and 11 weeks after crush (right). (B) Nerve conduction velocity (NCV), compound muscle action potentials (CMAPs) of the distal (C) and proximal (D) muscles of the operated ipsilateral (light brown bars) and the non-operated contralateral (white bars) sciatic nerves are shown as mean \pm SEM. Crush-injured wt (blue dots, $n = 8$) and Δ ETorA rats (orange dots, $n = 7$): NCV ($H = 35.5$, $p < 0.0001$), distal ($H = 35.62$, $p < 0.0001$) and proximal CMAPs ($H = 35.62$, $p < 0.0001$) of the ipsilateral sciatic nerves at 11 weeks after nerve crush compared to the recordings of the contralateral sciatic nerves and compared to sciatic nerves of naïve control wt (black dots, $n = 8$) or naïve control Δ ETorA (grey dots, $n = 8$) rats. Statistical analysis was done using the Kruskal-Wallis test with Dunn's multiple comparisons test. * $p < 0.05$; ** $p < 0.01$.

severity scores significantly by 68% in dystonic-like Δ ETorA rats (Fig. 8A,B). LFP recordings obtained approximately 10 min after discontinuing EP-DBS revealed a non-significant reduction of 15% in theta power of high frequency stimulated nerve-injured Δ ETorA rats compared to non-stimulated nerve-injured Δ ETorA rats (Fig. 8C). The delay was necessary for technical reasons and recordings during DBS were not possible due to large stimulation induced artifacts. Nissl staining of the post mortem tissue verified the correct positioning of the EP-DBS stimulating and recording electrodes (Fig. 8D,E).

4. Discussion

We provide evidence that wt and Δ ETorA rats recover differently from a denervation injury. Nerve conduction measures proved in both genotypes a comparable degree of axonal damage of the sciatic nerve weeks after the trauma. During the first weeks, when nerve function was still compromised, both wt and Δ ETorA rats developed DLM, such as hindlimb retraction or clenching during tail suspension. We considered these movements as lesion-induced "pseudodystonia", also found in patients with a proprioceptive loss due to deafferentation of various causes (Albanese et al., 2013; Berlot et al., 2019). Wt animals recovered from this phenomenon completely by week 9. In contrast, Δ ETorA rats

continued to exhibit abnormal focal hindlimb postures, which tended to spread to adjacent limbs in some animals until the experiment was terminated after 12 weeks. We sought to validate the observed DLM phenotype by quantitative kinematic analyses and classification, implementing a pipeline of deep learning algorithms. Interestingly, the most discriminatory features turned out to be partially reflective of the utilized DLM rating measuring right hindlimb retraction and toe clenching, but extending into the description of contralateral proximal and distal hindlimb kinematics. The dichotomized DLM score could be classified in an unbiased fashion by unsupervised cluster analysis in 85% of the rats. The motor phenotype could be adequately represented in the selected feature space with a classification accuracy of 0.85 using the SVC model and including the genetic background as a covariate. Furthermore, the genetic background of rats (at a late stage after nerve-injury) could be predicted accurately solely based on kinematic features and irrespective of their DLM score in an unsupervised cluster analysis as well as with a SVC model (85% classification accuracy each). The overall strength of this machine learning approach clearly lies in the conceptually plausible and algorithmically derived feature set, thereby promoting consistency and reproducibility across laboratories. Interestingly, kinematic studies of TOR1A patients revealed an abnormal degree of movement trajectory variability, a finding naturally

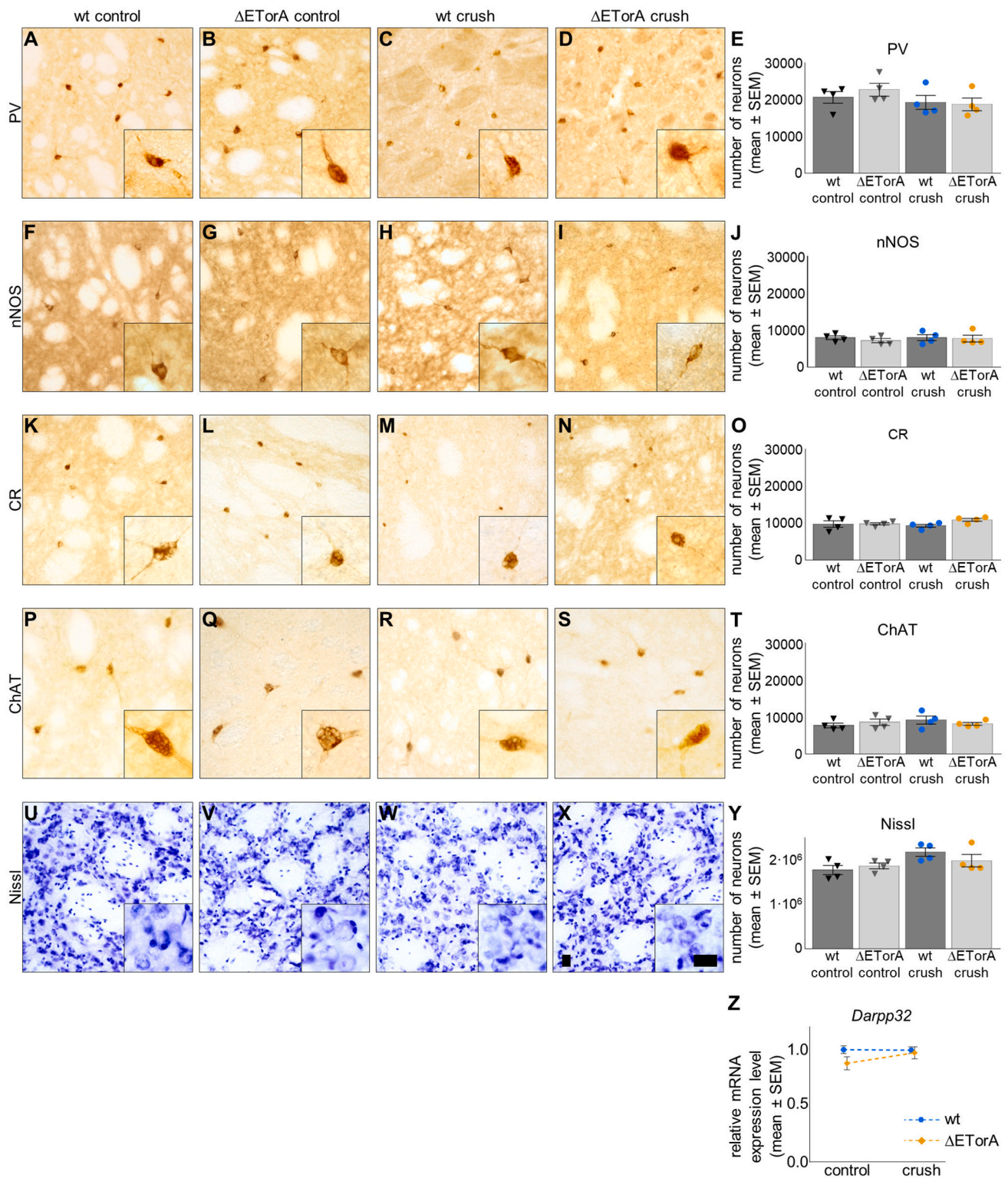
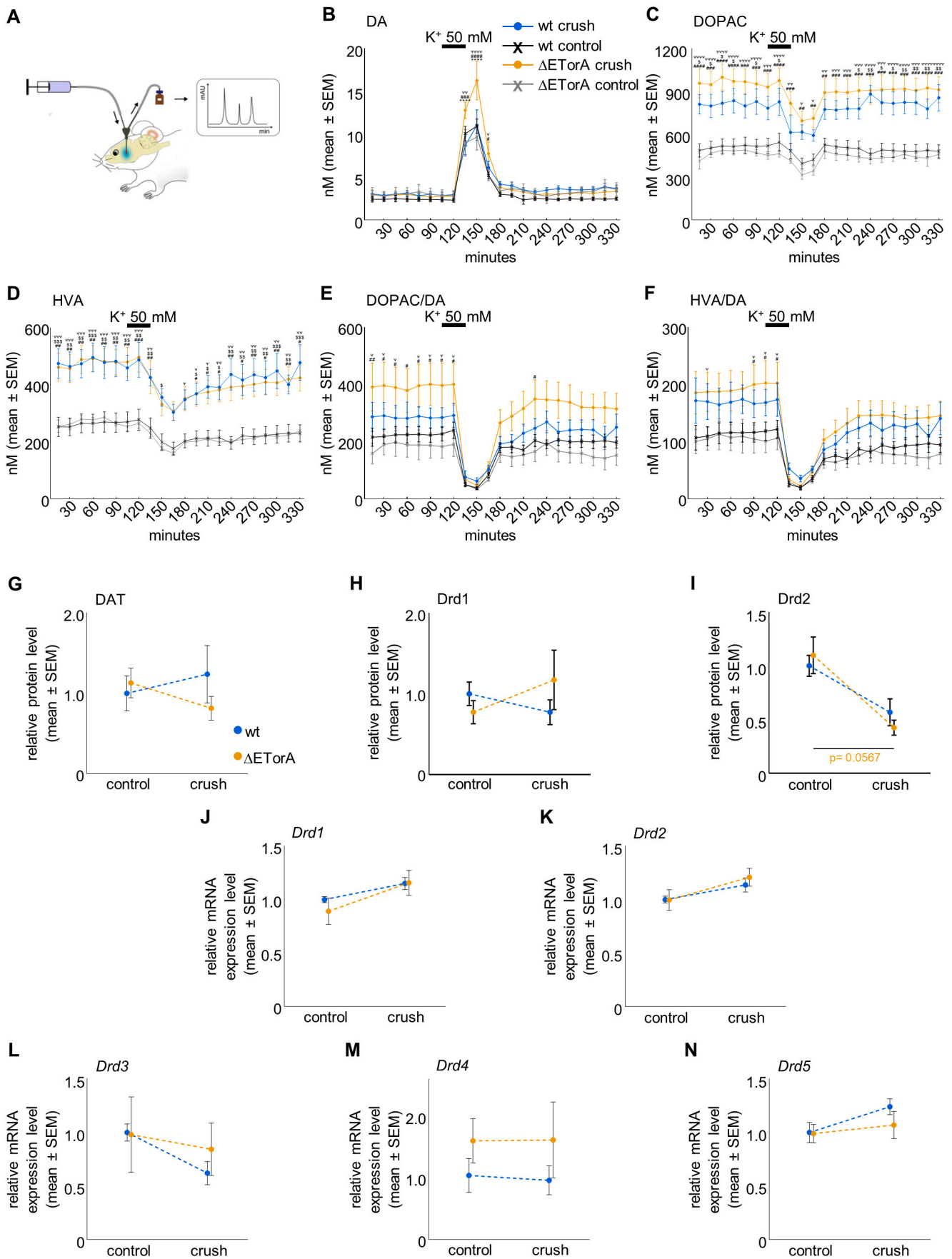


Fig. 5. No evidence of striatal neuronal cell loss in Δ ETorA rats.

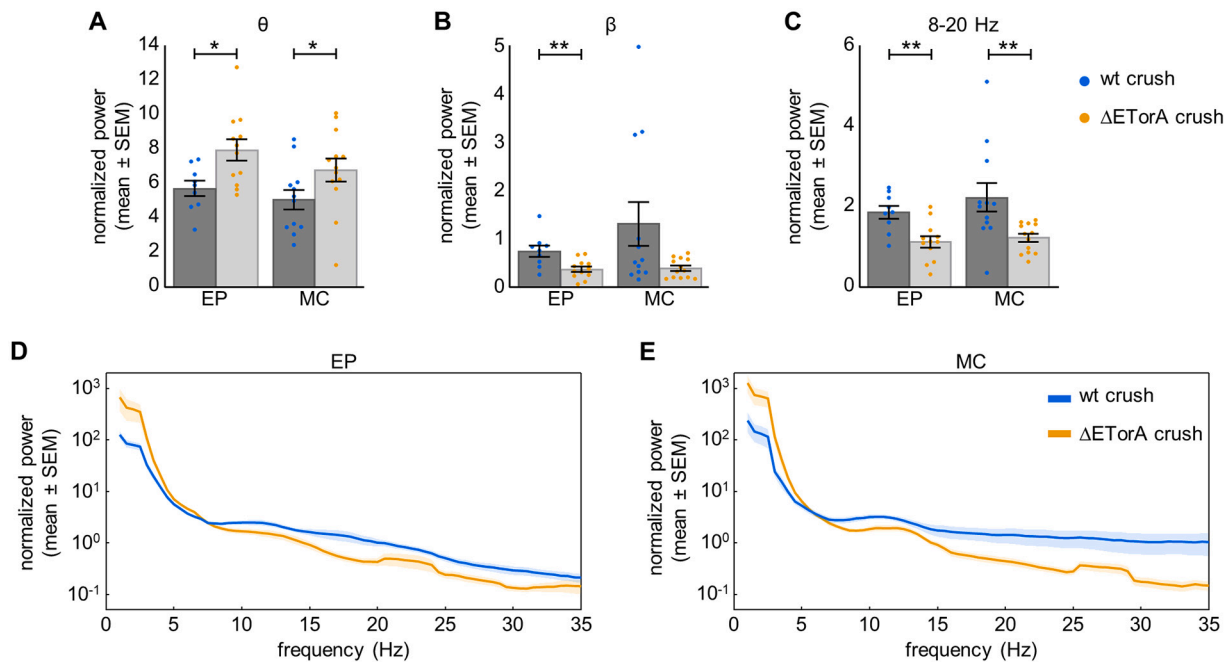
Representative images of immunohistochemically stained sections of striatal interneurons labeled for PV (A–D), nNOS (F–I), CR (K–N), ChAT (P–S) and Nissl stained striatal sections (U–X) of naïve control and crushed wt and Δ ETorA rats. Stereological quantification of the number of PV⁺ (E), nNOS⁺ (J), CR⁺ (O) and ChAT⁺ (T) interneurons and Nissl⁺ (Y) neurons in the striatum was performed in all four experimental groups 12 weeks after nerve crush injury (wt control: dark grey with black dots, $n = 4$; Δ ETorA control: light grey with grey dots, $n = 4$; wt crush: dark grey with blue dots, $n = 4$; Δ ETorA crush: light grey with orange dots, $n = 4$). Total number of neurons in the striatum are shown as mean \pm SEM. Statistical analysis was performed with one-way ANOVA and posthoc Tukey test. (Z) Striatal expression levels of *Darpp32* mRNA were investigated in wt (blue line; control: $n = 6$, crush: $n = 7$) and Δ ETorA rats (orange line; control: $n = 7$, crush: $n = 8$) before and 12 weeks after nerve crush injury. Data are shown as mean \pm SEM. Statistical analysis was performed using the Kruskal-Wallis test with Dunn's multiple comparisons test. Scale bars: 20 μ m.



(caption on next page)

Fig. 6. Elevated striatal DA metabolism in nerve-injured Δ ETorA rats.

(A) The schematic overview depicts the setup of the in vivo microdialysis perfusion of the striatum coupled with the HPLC analysis. Microdialysis perfusates of the striatum contralateral to the nerve crush were analyzed for DA (B: time main effect: $F_{21,373} = 113.4$, $p < 0.0001$; time \times groups interaction: $F_{63,373} = 3.270$, $p < 0.0001$), DOPAC (C: time main effect: $F_{21,374} = 24.21$, $p < 0.0001$; groups main effect: $F_{3,18} = 9.749$, $p < 0.0005$; time \times groups interaction: $F_{63,374} = 2.076$, $p < 0.0001$) and HVA (D: time main effect: $F_{21,374} = 61.89$, $p < 0.0001$; groups main effect: $F_{3,18} = 7.849$, $p < 0.01$; time \times groups interaction: $F_{63,374} = 2.629$, $p < 0.0001$) by HPLC comparing Δ ETorA rats and wt rats in control condition as well as 12 weeks after sciatic nerve crush. DA turnover rates measured by DOPAC/DA (E: time main effect: $F_{21,370} = 48.55$, $p < 0.0001$; time \times groups interaction: $F_{63,370} = 2.058$, $p < 0.0001$) and HVA/DA (F: time main effect: $F_{21,370} = 55.54$, $p < 0.0001$; time \times groups interaction: $F_{63,370} = 1.76$, $p < 0.001$) were calculated from these data. 90 min after experiment onset, highly concentrated potassium (K^+ 50 mM) was administered over a time period of 30 min as a depolarizing stimulus for neurotransmitter release. Values are shown as mean \pm SEM of wt crush (blue; $n = 5$), wt control (black; $n = 6$), Δ ETorA control (orange; $n = 7$) and Δ ETorA crush (grey; $n = 4$) rats. Statistical analysis was performed by using the mixed-effects model with Dunn's multiple comparisons test. ψ $p < 0.05$, $\psi\psi$ $p < 0.01$, $\psi\psi\psi$ $p < 0.001$, $\psi\psi\psi\psi$ $p < 0.0001$ wt control vs Δ ETorA crush; # $p < 0.05$, ## $p < 0.01$, ### $p < 0.001$, #### $p < 0.0001$ Δ ETorA control vs Δ ETorA crush; $\$$ $p < 0.05$, $\$\$$ $p < 0.01$, $\$\$\$$ $p < 0.001$ wt control vs wt crush; * $p < 0.05$, **** $p < 0.0001$ wt crush vs Δ ETorA crush. (G-I) Striatal protein levels of DAT (G), *Drd1* (H) and *Drd2* (I) were analyzed by western blot 12 weeks after sciatic nerve injury comparing naïve control and nerve-injured Δ ETorA rats (orange line; control: $n = 4-5$, crush: $n = 4-5$) and wt rats (blue line; control: $n = 4-5$, crush: $n = 5-6$). Gene expression levels of dopamine receptors encoded by *Drd1* (J), *Drd2* (K), *Drd3* (L), *Drd4* (M), *Drd5* (N) were determined in striatal tissue of wt (blue line; control: $n = 6$, crush: $n = 8$) and Δ ETorA (orange line; control: $n = 7$, crush: $n = 7$) rats before and 12 weeks after nerve crush injury. Data were normalized to wt control animals and are shown as mean values \pm SEM. Statistical analysis was performed with the Kruskal-Wallis test followed by Dunn's multiple comparisons test.

**Fig. 7.** Alterations of neuronal activity in nerve-injured Δ ETorA rats.

LFP recordings demonstrate theta power (A), beta power (B), and power in the frequency range of 8–20 Hz (C) assessed for baseline conditions 9 weeks after nerve crush injury in the contralateral EP and MC in nerve-injured wt (dark grey, dotted blue; EP: $n = 9$, MC: $n = 12$) and Δ ETorA (light grey, dotted orange; EP: $n = 12$, MC: $n = 13$) rats. Normalized power spectra of baseline recordings are shown for each genotype for EP and MC (D,E). Data are shown as mean \pm SEM. Statistical analysis was performed using non-parametric two-tailed Mann-Whitney test. * $p < 0.05$; ** $p < 0.01$.

encapsulated in our feature set (Sadnicka et al., 2019). This raises the question, to what extent “deep kinematic phenotyping” can open up avenues to establish common signatures of movement disorders in experimental and clinical setting allowing to improve stratification and to bridge translational gaps in neuroscience.

From a pathophysiological standpoint, the observed DLM postures obviously resulted from abnormal, sustained muscle contractions and overflow similar to human dystonia, but since no generally accepted clinical or electromyographic criteria allow to diagnose dystonic movements in humans and to distinguish dystonic movements from “pseudodystonia”, we could not validate the observed phenotype as dystonia per se. Instead, we set out to characterize central network changes in our animal model, which were known to accompany the clinical manifestation of dystonia in humans. We argued, that a similar endophenotype in dystonic patients and rats harboring the human TOR1A genotype, would provide the most convincing proof, that we were truly able to elicit dystonia in these animals by a peripheral nerve

trauma. Indeed, we found distinct alterations of striatal dopaminergic transmission and spectral changes of LFP recordings from the basal ganglia, which were neither observed in wt animals nor in Δ ETorA rats before the nerve crush, and were hence associated with the chronic manifestation of DLM in the genetically predisposed animals. Moreover, chronic HFS of the EP, the rat equivalent of the human GPI, effectively reduced the severity of DLM, corroborating their dependence on abnormal basal ganglia output.

Abnormal striatal DA signaling has long been suspected to play a role in dystonia pathophysiology. Autopsy studies of symptomatic TOR1A patients found an increased striatal DA turnover (Augood et al., 2002) and an enlargement of dopaminergic cell bodies in the substantia nigra compared to asymptomatic TOR1A mutation carriers or healthy subjects (Iacono et al., 2019; Rostasy et al., 2003). We have previously shown alterations hinting at a disturbed dopaminergic neurotransmission in response to nerve injury in *Tor1a*^{+/-} mice with a dystonia-like phenotype (Ip et al., 2016). Other TOR1A rodent models did not

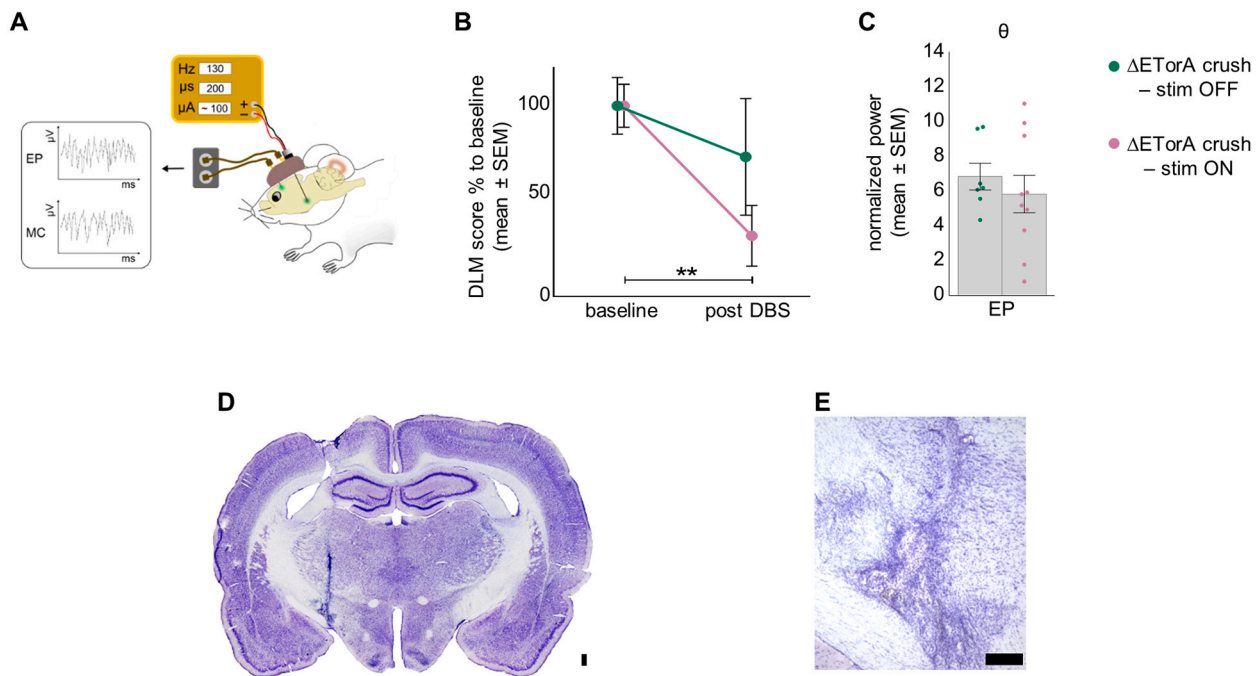


Fig. 8. Modulating effect on theta oscillation and amelioration of DLM by EP-DBS in Δ ETorA rats.

(A) The schematic overview illustrates the setup for HFS and LFP recordings. (B) 3 weeks after HFS of the EP, DLM scores were evaluated in non-stimulated (stim OFF; green; $n = 5$) and stimulated (stim ON; purple; $n = 8$), nerve-injured Δ ETorA rats. (C) LFP recordings of theta power in the contralateral EP were performed after 3 weeks of EP-DBS in nerve-injured Δ ETorA stim OFF (green; $n = 7$) and stim ON (purple; $n = 10$) rats. Representative image of the insertion channel of the unilateral EP-DBS microelectrode in the hemisphere contralateral to the nerve injury in a Nissl stained coronal whole-brain section (D) and at a higher magnification of the targeted EP (E). Data are shown as mean \pm SEM. Statistical analysis was performed using non-parametric two-tailed Mann-Whitney test. ** $p < 0.01$. Scale bars: 200 μ m.

exhibit a dystonia-like phenotype and only subtle or no striatal alterations in DA, HVA or DOPAC levels (Dang et al., 2005; Grundmann et al., 2007; Song et al., 2012). Likewise, we did not observe any differences in extracellular striatal DA level at baseline in Δ ETorA and wt rats; however, changes became apparent in nerve-injured Δ ETorA rats with the manifestation of DLM, such as a higher DA turnover with elevated HVA/DA and DOPAC/DA ratios. These observations could indicate a maladaptive plastic response of the striatal dopaminergic system to the nerve crush in Δ ETorA rats and are in line with the subtle metabolic changes previously described in TOR1A patients (Augood et al., 2002). Another proof of stress intolerance in nerve-injured Δ ETorA rats was the finding of markedly increased striatal extracellular DA levels after an acute potassium challenge compared to non-nerve-crushed Δ ETorA rats or wt control groups. In our previously analyzed *Tor1a*^{+/-} mouse model, administration of levodopa worsened DLM while treatment with a DA synthesis blocker reduced DLM, suggesting that a striatal over-availability of DA could trigger abnormal downstream signaling (Ip et al., 2016), similar to the dopaminergic mechanisms causing levodopa-induced dyskinesia in Parkinson's disease (Cenci and Crossman, 2018). Membrane depolarization induced by local potassium infusion is known to increase DA efflux; previous studies have revealed a reduction in striatal DA uptake in depolarized conditions due to internalization of DAT as a possible mechanism (Richardson et al., 2016; Woodward et al., 1986). It's known that torsinA influences DAT expression on the cell surface, which would in turn affect DA uptake and extracellular DA homeostasis (Torres et al., 2004). Interestingly, we found a trend towards reduced DAT levels after peripheral nerve crush in Δ ETorA rats contrasting wt rats with a slight DAT elevation. While postmortem studies with quantitative autoradiography revealed no differences in the DAT density, other TOR1A animal models reported DAT malfunction (Augood et al., 2002; Hewett et al., 2010; Ip et al., 2016).

Changes affecting the presynaptic release of DA have previously been described, with disturbed D1 and D2 receptor function reported in

different TOR1A animal models (Martella et al., 2014; Sciamanna et al., 2009; Yokoi et al., 2015). Previous work on this Δ ETorA rat model in its naïve state demonstrated no change in D2 receptor responsiveness on dopaminergic neurons using the D2-receptor agonist quinpirole (Grundmann et al., 2012). Our data did not reveal any differences in striatal DA receptor mRNA expression levels, however, striatal D2 receptor protein levels were robustly reduced in dystonic-like Δ ETorA rats, indicating a possible pathogenic role of the DA D2 receptor in this model. In line with this finding, a reduced D2 receptor protein level was observed in the striatum of juvenile TOR1A mice (*Tor1a*^{+/-}) that was induced by an increased lysosomal degradation (Bonsi et al., 2019). Altered dopaminergic release could also be due to an impaired GABAergic neurotransmitter system, which has been suggested by a PET study in TOR1A and sporadic dystonia patients and in *dt*^{SZ} dystonic hamsters (Garibotto et al., 2011; Hamann and Richter, 2002). The cholinergic system might also play a part in the uncontrolled DA efflux as both neurotransmitter systems are tightly intertwined. Moreover, anticholinergic medication reduces symptoms in dystonia patients (Fahn, 1983). Previous electrophysiological studies in Δ ETorA rats and in TOR1A knock-in mice showed an impaired long-term depression and synaptic depotentiation in medium spiny neurons, which were rescued by muscarinic receptor M1 antagonist, pointing at a pivotal role of the cholinergic system (Grundmann et al., 2012; Martella et al., 2014; Martella et al., 2009). Sciatic crush injuries can lead to transient pain, as shown by chronic constrictive injury (CCI) of the sciatic nerve in rats leading to thermal hyperalgesia that gradually resolved by 9 weeks (Kingerly et al., 1994). As CCI was shown to induce more pronounced and prolonged pain than a nerve crush injury (Attal et al., 1994), it is rather unlikely that pain is the primary cause of changes in DA metabolism observed in crush-injured Δ ETorA since DA measurements were performed 12 weeks post nerve crush and because all animals received appropriate analgesia. The elevated striatal dopaminergic metabolism in Δ ETorA rats 12 weeks after nerve injury strengthens our assumption,

since decreased striatal levels of DA were found in a mouse model for neuropathic pain and reduced DA levels are suggested to likely contribute to pain in human patients (Taylor et al., 2014; Wood, 2008). In summary, the observed alterations in striatal dopaminergic neurotransmission provide a proof of a maladaptive change within basal ganglia circuits in response to a peripheral trauma in Δ ETorA rats, but are just a starting point for further mechanistic research, rather than a full explanation of the underlying molecular or cellular pathways.

Abnormal oscillatory activity has been a focus of physiological research characterizing central motor network disorders of basal ganglia origin. These studies were possible by using chronically implanted electrodes in patients undergoing DBS as recording probes of LFP activity within basal ganglia nuclei. Increased power and reduced suppressibility of beta oscillations are a hallmark of the parkinsonian state, whereas lower frequency oscillations in the theta range have been found in hyperkinetic disorders such as levodopa-induced dyskinesia (Alegre et al., 2012), tics (Neumann et al., 2018) or dystonia (Liu et al., 2008; Sharott et al., 2008). The causal relationship of these oscillations to motor symptom manifestation remains a matter of debate, but they seem to be robust markers of symptomatic motor states (Chen et al., 2006; Kuhn et al., 2009) and correlate with therapeutic responses (Barow et al., 2014; Kuhn et al., 2008), in particular the motor improvement associated with DBS. Here, we provide a first description of spectral LFP changes recorded from rat motor cortex and basal ganglia associated with the evolution of dystonia-like motor symptoms. The observed changes closely resemble the “prokinetic” changes in LFP rhythms described in humans (Alegre et al., 2012; Sharott et al., 2008). In addition, sensory-related modulation of spectral power induced by vibration was represented by reduced GPi LFP power in the range of 8–20 Hz in dystonia patients (Liu et al., 2008). In keeping with this observation, by analyzing this specific frequency range, we observed a significant reduction of LFP power in nerve-injured Δ ETorA rats over wt controls, thereby potentially reflecting the disturbed sensorimotor integration in nerve-injured Δ ETorA rats.

We also found a trend for reduced low-frequency oscillations after a prolonged period of HFS within the EP, along with a significant reduction of DLM scores. This similarity with the clinical and physiological response to pallidal DBS in human dystonia further strengthens the validity of our rodent dystonia model. Of note, isoflurane anaesthesia was shown to suppress LFP power in a dose-dependent fashion (Tsurugizawa et al., 2016). However, by adjusting the isoflurane dose to comparable levels in all groups of animals and by conducting analgesation rather than deep anaesthesia, we tried to minimize and control the influence of anaesthesia on LFP results. In particular, anaesthesia should not present a major confound of the differential group analysis. If any change, we would expect an even stronger theta signal and therefore more robust group differences in awake animals based on the published attenuation of GPi theta power under general anaesthesia in dystonia patients (Moll et al., 2014). In addition, prominent LFP theta activity was described in cervical dystonia patients during generalized anaesthesia (Trenado et al., 2016), thereby supporting the notion that development of pathological oscillatory activity does not necessarily require an awake state and presence of dystonic movements. As such, our experimental setup to record anesthetized rodents is in line with published human studies (Trenado et al., 2016).

Physical trauma has long been suspected to contribute to dystonia pathophysiology, but the overall incidence of peripheral posttraumatic dystonia (PPD) in the general population is very low (Frei, 2017; Macerollo et al., 2019). PPD is diagnosed clinically, if the suspected trauma was severe enough to cause local symptoms for at least 2 weeks and dystonia evolves within 1 year at an anatomical location consistent with the injury (Krauss and Jankovic, 2002). Only 23 out of 3500 cases in dystonia database fulfilled the criteria for posttraumatic peripheral movement disorders (Jankovic and Van der Linden, 1988). The low prevalence in addition to other problems in defining PPD such as recall bias, legal ramifications and the lack of physical traces of injury at the

time of dystonia onset (often raising suspicion for psychogenesis), have led many movement disorders neurologists to doubt its existence at all (Frei, 2017). Nevertheless, cases of PPD have continuously been reported following the original description of Schott (Schott, 1985) and mild trauma such as repetitive strain injury has been implicated in the pathogenesis of writer’s cramp or musician dystonia (Byl, 2003). Here we provide experimental evidence that genetic (TOR1A) predisposition and physical trauma may act in concert to generate dystonia, thereby supporting the “two-hit” hypothesis for dystonia development (Kumar and Jog, 2011). In addition, our data indicates that the “two-hit” concept of gene-environment interaction might also have implications for the penetrance of dystonia. A reduced penetrance of 30–40% is known for human TOR1A dystonia, which has so far been explained by genetic modifiers such as the D216H polymorphism of the TOR1A gene leading to reduced risk for developing dystonic symptoms in gene carriers with the H allele (Kamm et al., 2008; Kock et al., 2006). However, since the H allele is rare with a frequency of 12–19% the D216H polymorphism does not explain the reduced penetrance in TOR1A patients entirely (Kamm et al., 2008; Kock et al., 2006) and indicates the existence of additional extragenic modifiers. In our controlled experimental environment, the penetrance of DLM in Δ ETorA at 9–12 weeks’ time point was high with 75%. It is therefore attractive to assume that some TOR1A mutation carriers might never develop manifesting dystonia without encountering a “second hit”. Underlining this assumption, a reduced penetrance was also observed in other monogenic dystonia such as DYT-THAP1 and DYT-GNAL (Dulovic-Mahlow et al., 2019; Vemula et al., 2013; Zorzi et al., 2018), thereby suggesting a similar gene-environment interaction affecting the penetrance of these diseases.

In conclusion, the value of this new model of dystonia lies in the ability to dissociate the endophenotype resulting from the Δ ETorA mutation and network changes associated with the manifestation of dystonia after the nerve injury. This will now allow targeted interventions in order to map the mechanisms of dystonia along the entire path from molecular to system network level.

Supplementary data to this article can be found online at <https://doi.org/10.1016/j.nbd.2021.105337>.

CRediT authorship contribution statement

Susanne Knorr: Methodology, Validation, Formal analysis, Investigation, Writing - original draft, Visualization, Project administration. **Lisa Rauschenberger:** Writing - original draft, Investigation. **Uri Ramirez Pasos:** Investigation, Writing - original draft. **Maximilian U. Friedrich:** Investigation, Writing - original draft. **Robert L. Peach:** Software, Validation, Writing - review & editing. **Kathrin Grundmann-Hauser:** Resources, Writing - review & editing. **Thomas Ott:** Resources, Writing - review & editing. **Aet O’Leary:** Investigation. **Andreas Reif:** Writing - review & editing. **Philip Tovote:** Writing - review & editing. **Jens Volkmann:** Writing - review & editing. **Chi Wang Ip:** Conceptualization, Methodology, Writing - review & editing, Supervision, Funding acquisition.

Declaration of Competing Interest

The authors declare no competing financial interests.

Acknowledgments

This work was funded by the German Federal Ministry of Education and Research (BMBF DysTract to C.W.I.), partially by the Deutsche Forschungsgemeinschaft (DFG, German Research Foundation) Project-ID 424778381-TRR 295 (A06 to C.W.I.) and under the frame of EJP RD, the European Joint Programme on Rare Diseases and the European Union’s Horizon 2020 research and innovation programme under the EJP RD COFUND-EJP N° 825575 (EurDyscover), by the Nündel Foundation and by the Interdisciplinary Center for Clinical Research (IZKF) at

the University of Würzburg (N-362 to C.W.I and P.T.; Z2-CSP3 to L.R.; Z2-CSP13 to M.U.F.). We thank Keali Röhm, Veronika Senger, Heike Menzel and Louisa Frieß for their technical assistance as well as Helga Brünner for the animal care.

References

- Albanese, A., et al., 2013. Phenomenology and classification of dystonia: a consensus update. *Mov. Disord.* 28, 863–873.
- Alegre, M., et al., 2012. Subthalamic activity during diphasic dyskinesias in Parkinson's disease. *Mov. Disord.* 27, 1178–1181.
- Attal, N., et al., 1994. Behavioural pain-related disorders and contribution of the saphenous nerve in crush and chronic constriction injury of the rat sciatic nerve. *Pain.* 59, 301–312.
- Augood, S.J., et al., 2002. Dopamine transmission in DYT1 dystonia: a biochemical and autoradiographical study. *Neurology.* 59, 445–448.
- Balint, B., et al., 2018. Dystonia. *Nat Rev Dis Primers.* 4, 25.
- Barow, E., et al., 2014. Deep brain stimulation suppresses pallidal low frequency activity in patients with phasic dystonic movements. *Brain.* 137, 3012–3024.
- Berlot, R., et al., 2019. Pseudodystonia: a new perspective on an old phenomenon. *Parkinsonism Relat. Disord.* 62, 44–50.
- Bonsi, P., et al., 2019. RGS9-2 rescues dopamine D2 receptor levels and signaling in DYT1 dystonia mouse models. *EMBO Mol Med.* 11.
- Byl, N.N., 2003. What can we learn from animal models of focal hand dystonia? *Rev. Neurol. (Paris)* 159, 857–873.
- Carbon, M., et al., 2004. Microstructural white matter changes in carriers of the DYT1 gene mutation. *Ann. Neurol.* 56, 283–286.
- Carbon, M., et al., 2009. Abnormal striatal and thalamic dopamine neurotransmission: genotype-related features of dystonia. *Neurology.* 72, 2097–2103.
- Carbon, M., et al., 2011. Impaired sequence learning in dystonia mutation carriers: a genotypic effect. *Brain.* 134, 1416–1427.
- Cenci, M.A., Crossman, A.R., 2018. Animal models of l-dopa-induced dyskinesia in Parkinson's disease. *Mov. Disord.* 33, 889–899.
- Chen, C.C., et al., 2006. Oscillatory pallidal local field potential activity correlates with involuntary EMG in dystonia. *Neurology.* 66, 418–420.
- Conte, A., et al., 2019. The role of sensory information in the pathophysiology of focal dystonias. *Nat. Rev. Neurol.* 15, 224–233.
- Dang, M.T., et al., 2005. Generation and characterization of Dyt1 DeltaGAG knock-in mouse as a model for early-onset dystonia. *Exp. Neurol.* 196, 452–463.
- Dulovic-Mahlow, M., et al., 2019. Highly reduced penetrance in a family with a THAP1 nonsense mutation: role of THAP1 expression? *Parkinsonism Relat. Disord.* 65, 274–276.
- Fahn, S., 1983. High dosage anticholinergic therapy in dystonia. *Neurology.* 33, 1255–1261.
- Frei, K., 2017. Posttraumatic dystonia. *J. Neurol. Sci.* 379, 183–191.
- Garibotto, V., et al., 2011. In vivo evidence for GABA(A) receptor changes in the sensorimotor system in primary dystonia. *Mov. Disord.* 26, 852–857.
- Ghilardi, M.F., et al., 2003. Impaired sequence learning in carriers of the DYT1 dystonia mutation. *Ann. Neurol.* 54, 102–109.
- Grundmann, K., et al., 2007. Overexpression of human wildtype torsinA and human DeltaGAG torsinA in a transgenic mouse model causes phenotypic abnormalities. *Neurobiol. Dis.* 27, 190–206.
- Grundmann, K., et al., 2012. Generation of a novel rodent model for DYT1 dystonia. *Neurobiol. Dis.* 47, 61–74.
- Hamann, M., Richter, A., 2002. Effects of striatal injections of GABA(a) receptor agonists and antagonists in a genetic animal model of paroxysmal dystonia. *Eur. J. Pharmacol.* 443, 59–70.
- Hewett, J., et al., 2003. TorsinA in PC12 cells: localization in the endoplasmic reticulum and response to stress. *J. Neurosci. Res.* 72, 158–168.
- Hewett, J., et al., 2010. Function of dopamine transporter is compromised in DYT1 transgenic animal model in vivo. *J. Neurochem.* 113, 228–235.
- Iacono, D., et al., 2019. Hypertrophy of nigral neurons in Torsin1A deletion (DYT1) carriers manifesting dystonia. *Parkinsonism Relat. Disord.* 58, 63–69.
- Ip, C.W., et al., 2016. Tor1a+/- mice develop dystonia-like movements via a striatal dopaminergic dysregulation triggered by peripheral nerve injury. *Acta Neuropathol Commun.* 4, 108.
- Jankovic, J., Van der Linden, C., 1988. Dystonia and tremor induced by peripheral trauma: predisposing factors. *J. Neurol. Neurosurg. Psychiatry* 51, 1512–1519.
- Kamm, C., et al., 2008. Susceptibility to DYT1 dystonia in European patients is modified by the D216H polymorphism. *Neurology.* 70, 2261–2262.
- Kingery, W.S., et al., 1994. The resolution of neuropathic hyperalgesia following motor and sensory functional recovery in sciatic axonotmetic mononeuropathies. *Pain.* 58, 157–168.
- Kock, N., et al., 2006. Effects of genetic variations in the dystonia protein torsinA: identification of polymorphism at residue 216 as protein modifier. *Hum. Mol. Genet.* 15, 1355–1364.
- Krauss, J.K., Jankovic, J., 2002. Head injury and posttraumatic movement disorders. *Neurosurgery* 50, 927–939 (discussion 939–40).
- Kuhn, A.A., et al., 2008. High-frequency stimulation of the subthalamic nucleus suppresses oscillatory beta activity in patients with Parkinson's disease in parallel with improvement in motor performance. *J. Neurosci.* 28, 6165–6173.
- Kuhn, A.A., et al., 2009. Pathological synchronisation in the subthalamic nucleus of patients with Parkinson's disease relates to both bradykinesia and rigidity. *Exp. Neurol.* 215, 380–387.
- Kumar, H., Jog, M., 2011. Peripheral trauma induced dystonia or post-traumatic syndrome? *The Canadian Journal of Neurological Sciences.* 38, 22–29.
- Liu, X., et al., 2008. The sensory and motor representation of synchronized oscillations in the globus pallidus in patients with primary dystonia. *Brain.* 131, 1562–1573.
- Macerollo, A., et al., 2019. Peripheral trauma and risk of dystonia: what are the evidences and potential co-risk factors from a population insurance database? *PLoS One* 14, e0216772.
- Martella, G., et al., 2009. Impairment of bidirectional synaptic plasticity in the striatum of a mouse model of DYT1 dystonia: role of endogenous acetylcholine. *Brain.* 132, 2336–2349.
- Martella, G., et al., 2014. Regional specificity of synaptic plasticity deficits in a knock-in mouse model of DYT1 dystonia. *Neurobiol. Dis.* 65, 124–132.
- Martino, D., et al., 2013. Extragenetic factors and clinical penetrance of DYT1 dystonia: an exploratory study. *J. Neurol.* 260, 1081–1086.
- Mathis, A., et al., 2018. DeepLabCut: markerless pose estimation of user-defined body parts with deep learning. *Nat. Neurosci.* 21, 1281–1289.
- Moll, C.K., et al., 2014. Asymmetric pallidal neuronal activity in patients with cervical dystonia. *Front. Syst. Neurosci.* 8, 15.
- Nath, T., et al., 2019. Using DeepLabCut for 3D markerless pose estimation across species and behaviors. *Nat. Protoc.* 14, 2152–2176.
- Neumann, W.J., et al., 2017. A localized pallidal physiologic marker in cervical dystonia. *Ann. Neurol.* 82, 912–924.
- Neumann, W.J., et al., 2018. Pallidal and thalamic neural oscillatory patterns in tourette's syndrome. *Ann. Neurol.* 84, 505–514.
- Oostenveld, R., et al., 2011. FieldTrip: open source software for advanced analysis of MEG, EEG, and invasive electrophysiological data. *Comput. Intell. Neurosci.* 2011, 156869.
- Quartarone, A., Hallett, M., 2013. Emerging concepts in the physiological basis of dystonia. *Mov. Disord.* 28, 958–967.
- Richardson, B.D., et al., 2016. Membrane potential shapes regulation of dopamine transporter trafficking at the plasma membrane. *Nat. Commun.* 7, 10423.
- Risch, N.J., et al., 2007. Intragenic Cis and trans modification of genetic susceptibility in DYT1 torsion dystonia. *Am. J. Hum. Genet.* 80, 1188–1193.
- Rostasy, K., et al., 2003. TorsinA protein and neuropathology in early onset generalized dystonia with GAG deletion. *Neurobiol. Dis.* 12, 11–24.
- Sadnicka, A., et al., 2019. What can kinematic studies tell us about the mechanisms of dystonia? *Prog. Brain Res.* 249, 251–260.
- Schott, G.D., 1985. The relationship of peripheral trauma and pain to dystonia. *J. Neurol. Neurosurg. Psychiatry* 48, 698–701.
- Sciamanna, G., et al., 2009. Impaired striatal D2 receptor function leads to enhanced GABA transmission in a mouse model of DYT1 dystonia. *Neurobiol. Dis.* 34, 133–145.
- Sharott, A., et al., 2008. Is the synchronization between pallidal and muscle activity in primary dystonia due to peripheral afference or a motor drive? *Brain.* 131, 473–484.
- Smith, J.E., et al., 2015. Dynamics of the functional link between area MT LFPs and motion detection. *J. Neurophysiol.* 114, 80–98.
- Song, C.H., et al., 2012. Functional analysis of dopaminergic systems in a DYT1 knock-in mouse model of dystonia. *Neurobiol. Dis.* 48, 66–78.
- Taylor, A.M., et al., 2014. Correlation between ventral striatal catecholamine content and nociceptive thresholds in neuropathic mice. *J. Pain* 15, 878–885.
- Torres, G.E., et al., 2004. Effect of torsinA on membrane proteins reveals a loss of function and a dominant-negative phenotype of the dystonia-associated DeltaE-torsinA mutant. *Proc. Natl. Acad. Sci. U. S. A.* 101, 15650–15655.
- Trenado, C., et al., 2016. Local field potential oscillations of the globus pallidus in cervical and tardive dystonia. *J. Neurol. Sci.* 366, 68–73.
- Tsurugizawa, T., et al., 2016. Distinct effects of isoflurane on basal BOLD signals in tissue/vascular microstructures in rats. *Sci. Rep.* 6, 38977.
- Vemula, S.R., et al., 2013. Role of Gα(olf) in familial and sporadic adult-onset primary dystonia. *Hum. Mol. Genet.* 22, 2510–2519.
- Wood, P.B., 2008. Role of central dopamine in pain and analgesia. *Expert. Rev. Neurother.* 8, 781–797.
- Woodward, J.J., et al., 1986. Dopamine uptake during fast-phase endogenous dopamine release from mouse striatal synaptosomes. *Neurosci. Lett.* 71, 106–112.
- Yokoi, F., et al., 2015. Decreased dopamine receptor 1 activity and impaired motor-skill transfer in Dyt1 DeltaGAG heterozygous knock-in mice. *Behav. Brain Res.* 279, 202–210.
- Zorzi, G., et al., 2018. Diagnosis and treatment of pediatric onset isolated dystonia. *Eur. J. Paediatr. Neurol.* 22, 238–244.